Li et al. Geoscience Letters (2023) 10:45
https://doi.org/10.1186/s40562-023-00299-2

Geoscience Letters

RESEARCH LETTER Open Access

Near-surface atmospheric electric field changes through magnetic clouds via coronal mass ejections

Lei Li[1,2], Tao Chen[1*], Chao Shen[3], Shuo Ti[1], Shihan Wang[1,2], Chunlin Cai[1], Wen Li[1,2] and Jing Luo[1]

Abstract

The Earth's electrical environment is influenced by both external and internal driving factors. Internal driving factors include the global charging current produced by lightning storms, global aerosol concentrations and cloud coverage. External factors are caused by various space weather phenomena, including changes in the Sun's magnetic field, solar flares, coronal mass ejections, and ionization changes from high-energy particles from the Sun and galactic cosmic rays. This study focuses on the cosmic ray intensity changes observed at the OULU Station and the vertical atmospheric electric field changes observed at the Azores and Studenec stations during a solar activity event in September 2017. The results indicate that the atmospheric electric field at the two stations (Azores and Studenec) simultaneously decreased by 80% and 120% of the mean atmospheric electric field value, respectively, during the same time as the significant decrease in cosmic ray intensity. The linear correlation coefficient between the decreased atmospheric electric field measured at these two stations was 0.60, indicating a global effect from the shocks and magnetic clouds associated with coronal mass ejections on atmospheric electricity. Finally, this study describes shock waves and magnetic clouds that impede the propagation of galactic cosmic rays, resulting in a decrease in ionospheric potential and atmospheric electric field.

Keywords Coronal mass ejections, Atmospheric electric field, Cosmic ray intensity

Introduction

Coronal mass ejections (CMEs) indicate that large-scale plasma is ejected from the Sun into interplanetary space and is a major driver of space weather effects (energetic particles, shocks, and geomagnetic storms). CMEs can cause large disturbances in geomagnetic activity (Kamide et al. 1998; Yermolaev et al. 2014; Zhang et al. 2007) and other space weather effects (Kudela et al 2000; Sanchez-Garcia et al 2017; Lingri et al. 2016); they can also disturb the cosmic ray intensity (CRI) (Cane 1999; Oh et al. 2008). Galactic cosmic rays (GCRs) are energetic particles that originate from outside the solar system and consist mainly of protons, α particles and a few electrons, whose energy spectrum basically follows a power-law distribution and can reach energies of 10^{22} eV (Blasi 2013). GCRs are the main source of ionization in the atmosphere below 20 km, can cause direct and indirect space radiation events and are also significantly associated with space environment elements, such as the geomagnetic intensity (Bothmer and Daglis 2007; Guiming 2002).

Different time scales and intensities of plasma perturbations caused by solar activities can affect the propagation of GCRs in interplanetary space. Based on different modulation factors and time scales, this effect can be

*Correspondence:
Tao Chen
tchen@nssc.ac.cn
[1] State Key Laboratory of Space Weather, National Space Science Center, Chinese Academy of Sciences, Beijing 100190, China
[2] College of Earth and Planetary Sciences, University of Chinese Academy of Sciences, Beijing 100049, China
[3] School of Science, Harbin Institute of Technology, Shenzhen 518055, China

classified into many kinds, and the Forbush decrease is a sharp drop and gradual recovery in the flux of the Earth's GCRs caused by short-lived intense solar activities (Potgieter 2013; Kharayat et al. 2016). The Forbush decrease is a universal phenomenon within the heliosphere and has been observed on other planets (Guo 2018). The results from Lara et al. (2005) show that all CME properties have some correlation with the CRI, and the specific properties (width, velocity, or energy proxy) tend to have similar correlations with the CRI. In addition, based on the data of cosmic-ray electrons and positrons from the Dark Matter Particle Explorer, Alemanno et al. (2021) found that the Forbush decreased due to the solar event in September 2017. They described in detail the relationship between the CRI decrease and solar activities.

The near-surface vertical atmospheric electric field (E_z) is the electric field that is always present in the atmosphere due to the potential difference between the ionosphere and the Earth's surface, and the atmosphere between them is like a parallel plate capacitor of size 0.7 F. Under fair weather conditions (fair weather conditions suited for atmospheric electrical measurements, and they can be referred to Harrison and Nicoll (2018)), the resistance between them is about 200 Ω, and both air–earth current and E_z point vertically towards the ground, with air–earth current density and E_z being about 2 A•m^{-2} and 10^2 V/m, respectively. Then, there is a continuous charging of ionosphere from the Earth's surface through thunderstorms (~90%), electrified shower clouds (~9%) and rainfall (~1%), with a charging current magnitude of about 1250 A. The energy associated with the global atmospheric circuitry is enormous, at 2×10^{10} J, and the whole circuit is known as global atmospheric circuit (Rycroft et al. 2000, 2008). Based on global electric circuits, the finite conductivity of the atmosphere and E_z result from the presence of ions, generated by cosmic rays, and the decay processes from Earth's natural radioactivity near the surface (Harrison 2004). Due to this, solar activities can change the atmospheric conductivity, and the E_z can change by modifying the CRI and ionization of ions. To study the effect of solar activities on atmospheric electricity, Smirnov (2014) studied the effects of geomagnetic storms on the electrical parameters of the near-surface atmosphere in Kamchatka on April 5, 2010. The results showed that the air conductivity began to decrease 4 h before the geomagnetic storm, and potential gradient oscillations with amplitudes up to 300 V/m occurred at the beginning of the storm. Then, based on the long-term observations of electric and geomagnetic fields from the Borok Geophysical Observatory at mid-latitudes during the 1998–2015 period, Anisimov et al. (2021) studied the response of mid-latitude near-Earth atmospheric electric field variations in relation to strong magnetic storms. They counted 19 cases of strong and very strong magnetic storms corresponding to changes in the fair-weather atmospheric electric field. The statistical results showed an increase in the atmospheric electric field over a time interval of ± 4 h relative to the time of the minimum of the disturbance storm time (Dst) variation of the magnetic storm. Measurements of the fair-weather E_z can also be used to study the effects of solar events, such as solar flares and solar energetic particle events on global atmospheric circuits. Using superposed epoch analysis, Tacza et al. (2018) studied the atmospheric electric field data observed at Complejo Astronómico El Leoncito in San Juan, Argentina, during the period of January 2010 to December 2015. There was no deviation in the atmospheric electric field values after solar flares, and the atmospheric electric field increased by approximately 10 V/m after solar proton events. For the analysis of solar proton events and E_z, Shumilov et al. (2015) studied the relationship between three solar cosmic ray events and the atmospheric electric field observed at the Apatity High Latitude Observatory on April 15, April 18, and November 4, 2001. They showed that solar cosmic ray events caused perturbations in the atmospheric electric field.

Our conclusion in this study regarding the effects of CMEs on E_z differs from other studies, because interplanetary coronal mass ejections (ICMEs) propagating in interplanetary space can form shocks and magnetic clouds, which can block the propagation of GCRs. This process then causes a decrease in both the ionization of Earth's atmosphere and atmospheric E_z, rather than a perturbation of the E_z. This study focuses on an intense Forbush decrease event that occurred in September 2017. The E_z measured at two different surface stations and the CRI observation data observed at OULU Station were then analyzed. The correlation between the E_z decrease changes at these 2 stations and the physical mechanism of the shocks and magnetic clouds associated with CMEs on the E_z decrease were also studied and discussed.

Data

Most observations of CRI are made using data measured by neutron monitors, which are widely distributed around the world. These neutron monitors are mostly located in the middle and high latitudes, which are useful for studying the global distribution characteristics of cosmic rays. Compared with direct detection experiments, neutron monitors can only reflect an integral variation in the incident particle intensities; thus, much information regarding the compositions and precise energy spectra dependencies are lost (Anisimov et al. 2021). In our study, the CRI was measured via OULU's neutron monitors (65.05°N, 25.47°E; effective vertical geomagnetic cutoff

rigidity $R_c \sim 0.8$ GV, average count rate $N \sim 120\ s^{-1}$), and the temporal resolution of the data was 1 min.

Figure 1 depicts the geographical locations of two observation stations, Azores (AZO) Station (39.09°N, 28.03°W, altitude is 31 m) and Studenec (STU) Station (50.26°N, 12.52°E, altitude is 712 m), and both contain observations of atmospheric E_z. Figure 1 shows that the STU station is located inland in the Czech Republic, while the AZO station is situated on an island in Portugal. A comparison of the AZO and STU stations shows that both are located in mid-latitude regions, with an altitude difference of 681 m.

The AZO and STU stations use two different instruments to measure the E_z. The AZO station uses the JCI 131F instrument, which is capable of automatically selecting the measurement range of 2, 20, and 200 kV/m. It has a high accuracy of ± 1.5% of the measurement range, low noise, and a stable zero value. The STU Station uses the Boltek EFM 100 instrument, which automatically selects the measurement range of 5–20 kV/m. It has an accuracy of 5% of the reading value ± 0.05 kV/m. Their E_z observation data are publicly available from the following website: https://data.ceda.ac.uk. It is important to note that data from 16 other stations at this site were also studied, but they were excluded because of data loss and non-fair weather conditions.

Results

An ICME associated with a shock arrived at the Earth during the end hour of September 6th, 2017, and a worldwide Forbush decrease began. Figure 2 illustrates the variations in solar activity-related parameters and CRI during the period of September 1st–11th, 2017. Panels (a)–(f) represent the interplanetary magnetic field (IMF) in nT, its north–south component B_z in nT, solar wind speed V in km/s, dawn–dusk electric field E_y in mV/m, Dst index in nT, and CRI in counts/s as observed by the OULU neutron monitor, respectively. The time resolution of all physical parameters in Fig. 2 was 1 h.

During September 1st–11th, 2017, a shock (S1) associated with the first ICME (ICME1) of the interval arrived in the last hours of September 6th. This shock signature was evident in the IMF B_z, V, E_y, and Dst indices, and they all showed a sudden increase around the same time. The sheath region (Sheath l) followed this first shock S1 until approximately 20:00 UT on September 7th, and then ICME ejecta (CME1) arrived. While this ejecta was passing, a shock (S2) associated with the second ICME that arrived on September 7th at approximately 23:00 UT, followed by a sheath region (Sheath2) and ICME ejecta (ICME2). These shocks and ICMEs could also be observed on the following website: https://izw1.caltech.edu/ACE/ASC/DATA/level3/icmetable2.htm.

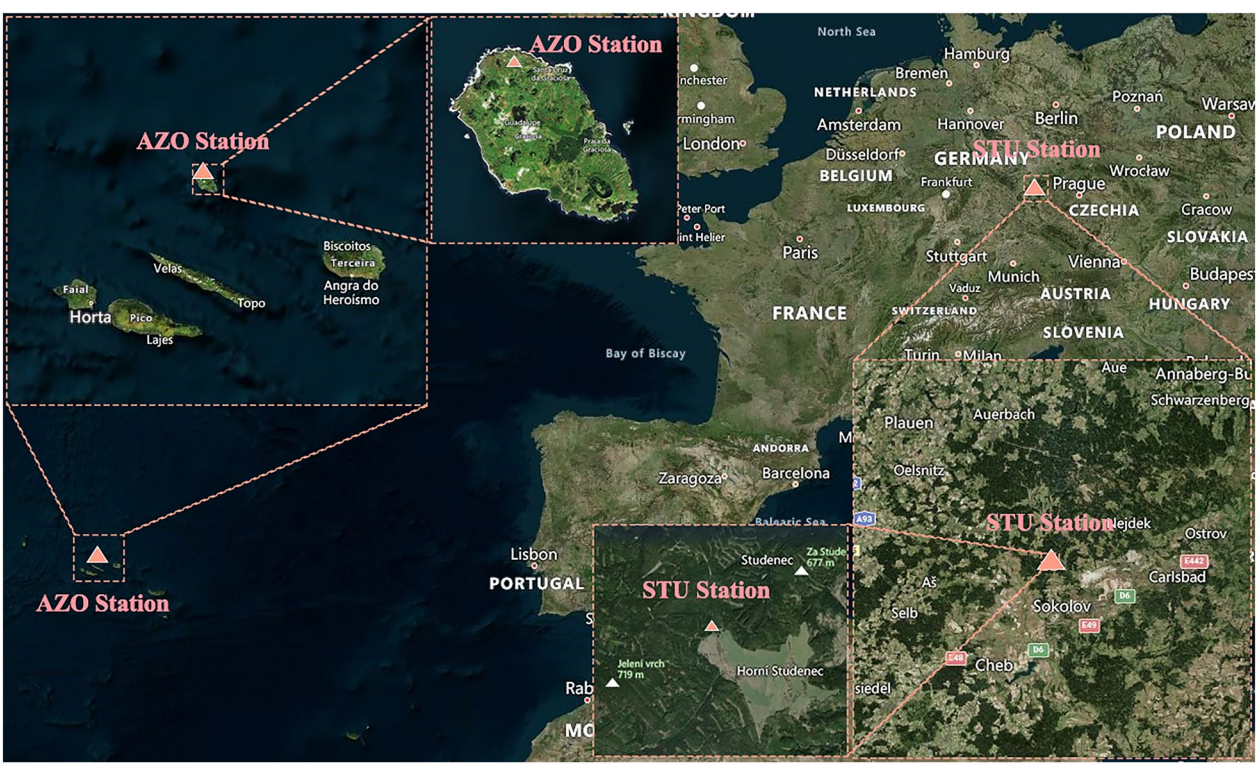

Fig. 1 Maps at different magnification scales for the AZO and STU stations

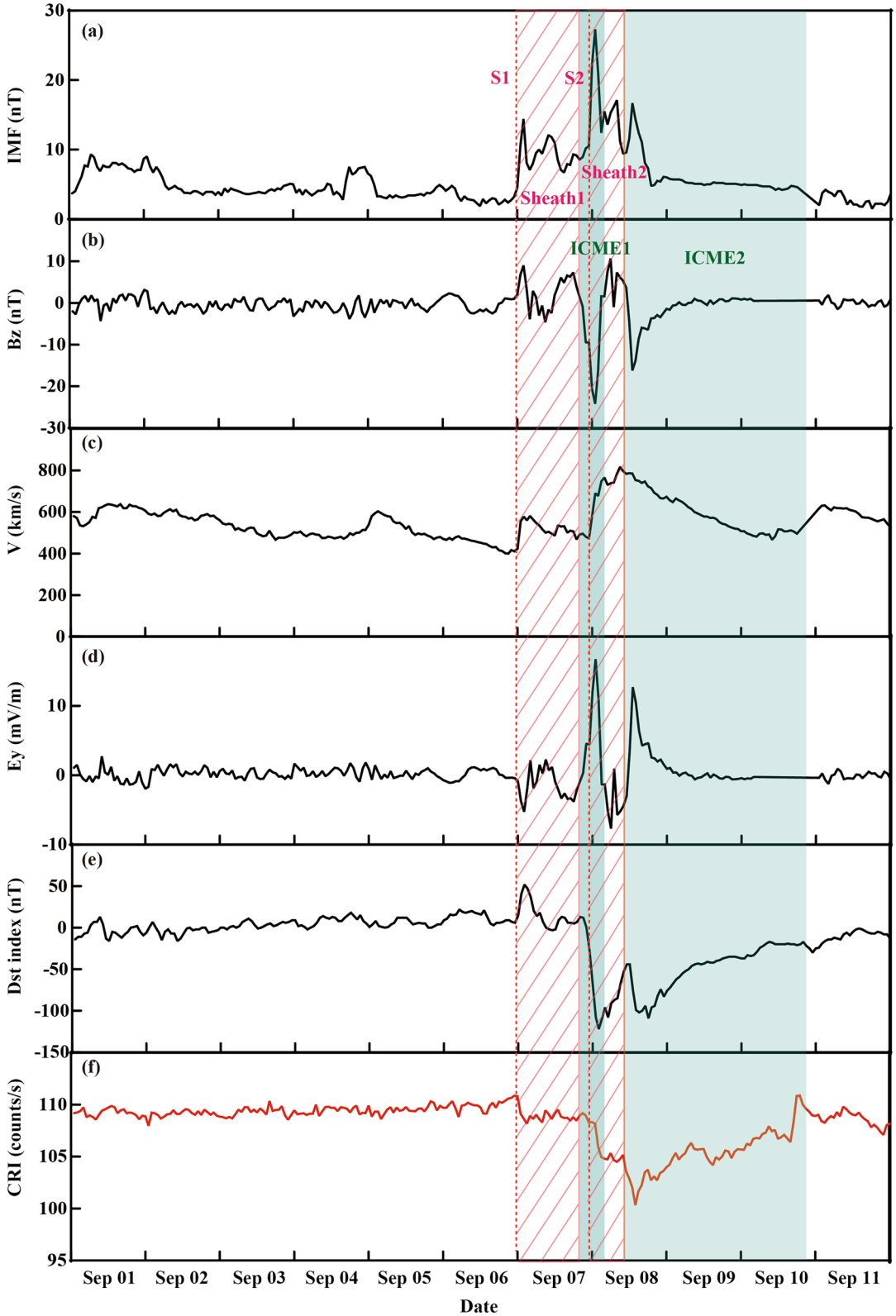

Fig. 2 Hourly variation in the related physical parameters during the period of September 4th–10th, 2017 (cosmic ray intensity by the OULU neutron monitor (panel **f**, counts/s), Dst index (panel **e**, nT), interplanetary magnetic field magnitude IMF (panel **a**, nT), north—south component of the interplanetary magnetic field B_z (panel **b**, nT), solar wind velocity V (panel **c**, km/s), and dawn–dusk electric field E_y (panel **d**, mV/m), S1 and S2 mean Shock1, Shock2)

In panel 2(f), the CRI 1-h averaged values observed by the OULU neutron monitor remained between 105 and 115 counts/s during the normal period of September 1st–6th. However, after the occurrence of S1, the CRI decreased to approximately 108 counts/s and then stabilized. During the passage of ICME1 ejecta on September 8th at 01:00 UT, the CRI showed a significant drop, reaching a minimum of 100.34 counts/s on September 8th at 13:00 UT. Over the next 3 days, the CRI gradually increased and returned to normal levels.

Both solar events (S1, S2, ICME1 and ICME2) were due to coronal mass ejections emanating from sunspot group AR2673. The first solar event was associated with the M5.5 flare on September 4th, and the second was associated with the X9.3 flare on September 6th (the most intense flare in solar cycle 24). The southward magnetic field contained in ICME1 was amplified by S2, which enhanced the geomagnetic storm.

Figure 3 provides a higher time resolution of the ICME and near-Earth structures through the details of different parameter fluctuations at different stages. In the upper right corner of Fig. 3, the CRI observed by the OULU station throughout September 2017 is shown. The changes in CRI from September 7th–10th are magnified in the middle of Fig. 3. Unlike in Fig. 2, the time resolution of CRI in Fig. 3 is 1 min. Based on Fig. 3, the CRI observed by the OULU station was normally maintained between 102 and 110 counts/s, similar to the trend shown in Fig. 2f. However, there was a clear decrease in the CRI at approximately 00:00 UT on September 8th, followed by a second decrease at approximately 10:00 UT on the same day, which was related to the arrival of S2.

To study the effect of solar activities on the E_z, it was necessary to first eliminate E_z observations under disturbed weather conditions and ensure that the E_z observation was reliable and standardized. Ultimately, only E_z measurements at the AZO Station and STU Station on September 8th–9th met these requirements. We strictly follow the fair weather criteria of Harrison and Nicoll (2018): maximum relative humidity < 95%, wind speed < 8 m/s, no precipitation, no low stratiform cloud. The weather data we used in this study can be viewed on the website: https://www.wunderground.com. Unfortunately we do not have access to cloud data and we have to execute other criteria. Then, the nearest meteorological observation to AZO Station is 2.4 km from the station and it is 39.1 km for STU Station. As shown in Fig. 4, the numbers in parentheses indicate average values of the variation of this meteorological parameter. It can be seen that the range of temperature, relative humidity and wind speed were 13–18 ℃, 53–83%, 1.1–6.1 m/s at AZO Station during September 8–9th, 2017. Average wind speed at AZO Station was 3.2 m/s. In addition, for STU Station, the range of temperature, relative humidity and wind speed were 5–11 ℃, 59–94%, 0.6–4.7 m/s during September 8th–9th and average wind speed was 2.2 m/s.

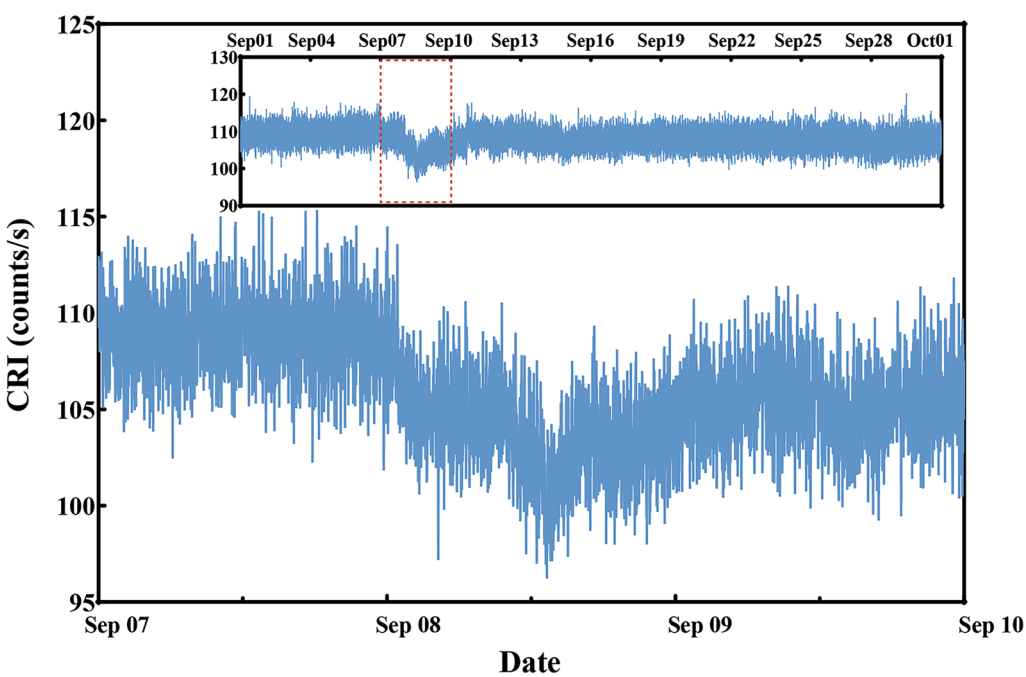

Fig. 3 Neutron detector measurements of cosmic ray intensity at OULU Station (top right corner shows the cosmic ray intensity for September 2017, the middle panel zooms in on the cosmic ray intensity from September 7th–9th with a time resolution of 1 min)

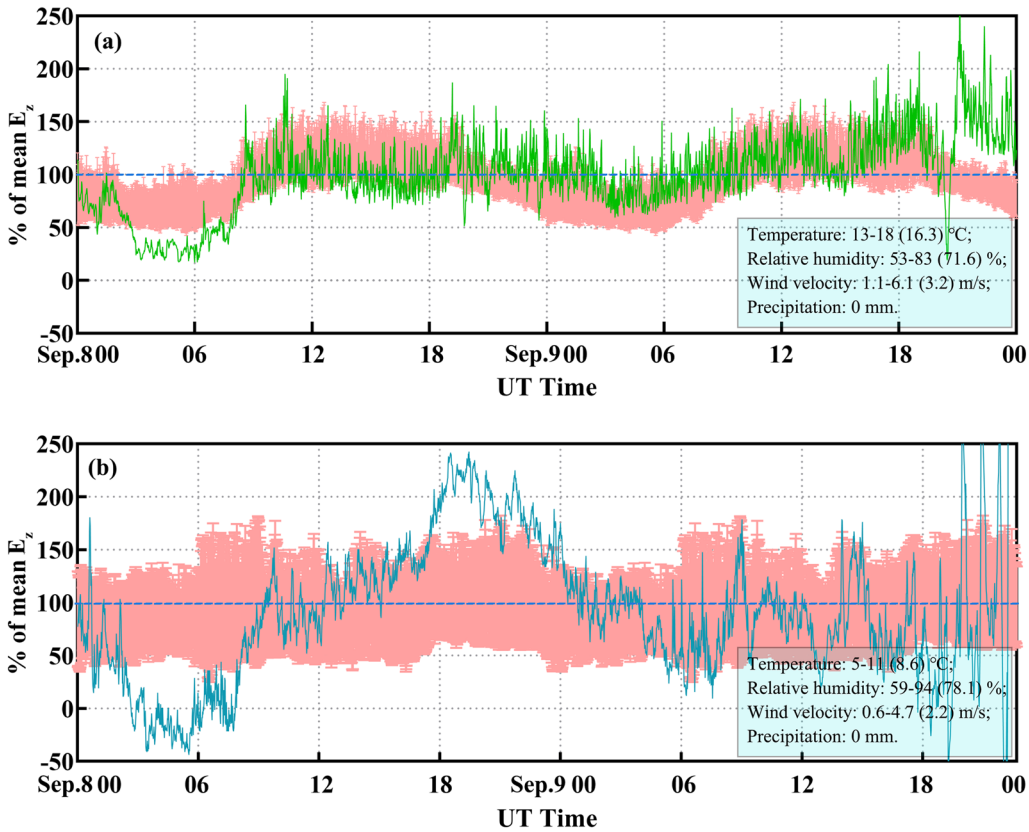

Fig. 4 Changes in E_z measured at AZO and STU stations from September 8th–9th, 2017 (panels **a** and **b** show the measurement results for the AZO and STU stations, respectively, with a time resolution of 1 min, the vertical axis represents the atmospheric electric field divided by the mean atmospheric electric field, and the pink background lines represent the upper and lower quartiles (25%, 75%) of the atmospheric electric field during other clear sky periods in September. Then, values in the box at bottom right are variations of meteorological parameters, and the numbers in parentheses indicate average values)

The precipitation at these two stations remained constant at 0 mm during this period and they met the fair weather criteria.

Their relative curve changes in E_z on September 8th–9th are shown in Fig. 4; the average E_z value was considered 100% and the time resolution of the E_z data was 1 min. Panels (a) and (b) correspond to the E_z observations at the AZO and STU stations, respectively, with the UT time on the horizontal axis. To compare their changes on those days with the background changes, the E_z observations for all other sunny days for the station in September 2017 were statistically analyzed for each moment, and the upper and lower quartiles (75% and 25%) were plotted as the pink background lines in the figure.

Mean E_z value (100%) in Fig. 4a (AZO Station) and b (STU Station) is 128.70 V/m and 11.28 V/m, respectively. In Fig. 4a, the E_z exhibited a clear decrease below the background level from the beginning of September 8th, there was one fluctuation at approximately 03:00 UT, and the average E_z value reached a trough of 19.4%. The E_z stabilized at 20–40%, then significantly increased at approximately 06:00 UT and recovered to the normal level. Figure 4b is similar to Fig. 4a; at the beginning of these two curves, the E_z showed a clear decrease below the background level from the beginning of September 8th and reached a trough of − 21.3% at approximately 03:00 UT. The E_z then stabilized at − 50% to 0% for approximately 3 h, significantly increased at approximately 06:00 UT and recovered to the normal level.

Comparing the observations of the two stations, the average E_z value at AZO Station during this period was 10 times higher than STU Station; the difference could be related to their geographical environment. Based on the results in Fig. 4, it was apparent that the fluctuations at STU Station were more pronounced during the period of significant CRI decrease, but the amplitude of the E_z fluctuations at STU was approximately 14 V/m, while it was approximately 105 V/m at AZO Station, which could be related to the underground radioactive substance content. Overall, the E_z observed at both the AZO and STU stations decreased significantly during the CRI period,

but they recovered faster than the CRI after the decrease. Notably, the E_z at both stations later increased significantly, which was potentially related to the recovery phase of CRI; however, from Fig. 4, these events did not occur synchronously, which would need further investigation in future research.

To demonstrate that the descending portions of the E_z curves for the AZO and STU stations reflected the same physical process, we extracted these two portions and normalized them. We then performed a correlation analysis on these normalized curves, as shown in Fig. 5. Figure 5a shows the time-delay correlation graph, with a maximum correlation coefficient of $R = 0.77$ corresponding to a time delay of 0 min. This result indicated that the two curves were synchronous. We then conducted a linear correlation analysis on these two curves, as shown in Fig. 5b. In Fig. 5b, the horizontal and vertical axes represent the E_z observations for the AZO and STU stations, respectively. The scatter plot of these observations is shown as the small black dots, and the red line is the linear regression line. The resulting correlation coefficient between these two stations was $R^2 = 0.60$. This indicated that the E_z anomaly observed at the AZO and STU stations on September 8th, 2017, reflected the same physical phenomenon.

In general, after the CME eruption, ICME1-related shocks propagated through interplanetary space and arrived during the last hour of September 6th, 2017. Subsequently, the IMF, B_z, solar wind speed, dawn–dusk electric field, and Dst index all exhibited significant fluctuations. Prior to the arrival of ICME1, the CRI observed by the OULU station showed a slight decrease. On September 8th, a significant decrease in CRI was observed, and in addition, the E_z values observed by the AZO and STU stations further showed synchronous decreases. However, after reaching their minimum levels, the E_z values remained at this level for only approximately 3 h before beginning to recover to normal levels. The CRI reached its minimum value at approximately 10:00 UT on September 8th, then quickly began to recover; and took approximately 3 days to return to normal levels.

Conclusions and discussion

In summary, this work compared the potential gradient and cosmic ray intensity with solar wind data for a high solar activity period in September 2017. ICME1-related shocks arrived during the last hour of September 6th, causing a decrease in the CRI observed by the OULU neutron monitor. After the arrival of ICME1, the E_z curves measured by the AZO and STU stations also exhibited different magnitudes of decrease, with reductions of 80% and 120% relative to the average E_z value, respectively. The E_z value at the AZO station decreased by approximately 105 V/m, which is approximately 90 V/m higher than that observed at the STU station. Unlike the AZO Station, the E_z value at the STU Station dropped below zero. Through correlation analysis, the E_z anomalies observed at the AZO and STU stations during the decrease and recovery phases were found to be significantly correlated with a coefficient of 0.60 and a lag time of 0 min, indicating a global effect on near-surface atmospheric electricity.

Based on Ohm's law, the E_z in the atmosphere depends on the ionization of ions in the atmosphere and fair-weather atmospheric current (Sun, 1987). The ionization of ions in the low atmosphere depends on the concentration of radioactive gases, such as radon in the crust. At high altitudes, cosmic rays can change the degree of ionization in the atmosphere. If the influx of cosmic rays increases, more ions will be ionized. The physical mechanism of the shock and magnetic cloud associated with CME effect on the near-surface E_z is shown in Fig. 6. Figure 6a shows the global atmospheric circuit under normal conditions, while panel (b) is shown under the effect of the shock and magnetic cloud associated with CME. The shock wave and magnetic cloud obstructs the propagation of CGRs, resulting in fewer CGRs that can enter the Earth's atmosphere. This process leads to a significant decrease in the electric potential of the ionosphere; as the distance between the bottom of the ionosphere and the Earth's surface remains constant, the E_z exhibits a significant decrease. In addition, since the resistance between the ionosphere and the Earth's surface is constant, the fair-weather atmospheric current between the ionosphere and the Earth's surface is weaker; also, to meet the circulation of the global atmospheric circuit, the thunderstorm current is weaker.

A variety of space weather-related phenomena, such as CMEs, can modify the ionization rate and, therefore, affect atmospheric conductivity. Due to this, the impact of different solar activity events on the near-Earth atmospheric electricity varies (Nicoll 2014), and the underlying details and physical mechanisms warrant further investigation and discussion. In the future, comprehensive observational instruments, including the E_z, atmospheric conductivity meters, positive and negative ion concentration sensors, meteorological parameters, and radioactive gas detectors, can be used to comprehensively observe multiple physical quantities. These observations can aid in the determination of the physical correlations among these phenomena.

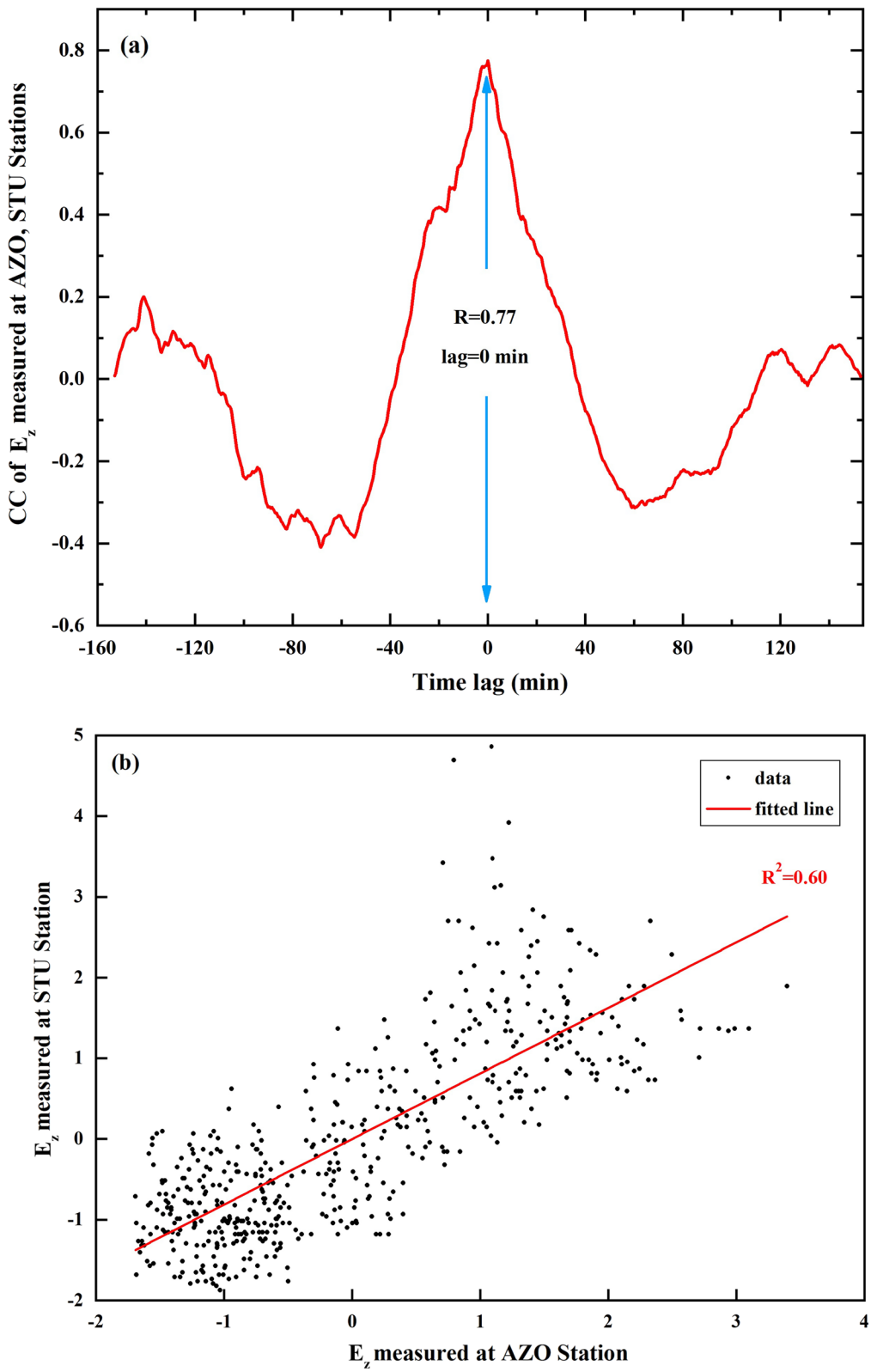

Fig. 5 Correlation of abnormal decrease and recovery segments of E_z measured at AZO and STU stations

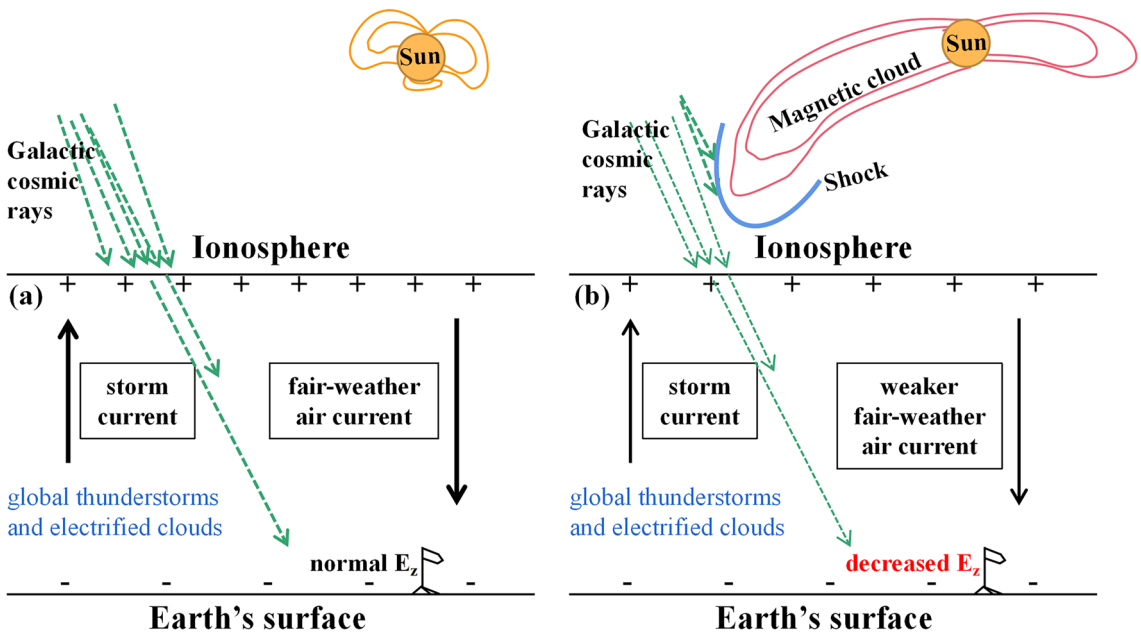

Fig. 6 Schematic diagram of global atmospheric electric circuit under normal and abnormal conditions (panel **a** presents the global atmospheric electric circuit under normal condition, while panel **b** indicates it during coronal mass ejection)

Abbreviations

CMEs	Coronal mass ejections
CRI	Cosmic ray intensity
GCRs	Galactic cosmic rays
E_z	Atmospheric electric field
ICMEs	Interplanetary coronal mass ejections

Acknowledgements
The authors would like to thank National Centre for Atmospheric Science and National Centre for Earth Observation (https://catalog.ceda.ac.uk) for providing atmospheric electric field and other open websites for providing the data sets of other parameters.

Author contributions
TC conceptualized this study. LL processed and analyzed the data. LL prepared the original draft, with contributions from all authors. CS, CC, ST, SW, WL and JL contributed to the discussion. All authors have read and approved the final manuscript.

Funding
This research was funded by the National Natural Science Foundation of China (Grant Nos. 42130202 and 41931073). The authors thank the International Partnership Program of Chinese Academy of Sciences (Grant No. 183311KYSB20200003), Strategic Pioneer Program on Space Science, the Chinese Academy of Sciences (Grant No. XDA15350201), Pandeng Program of National Space Science Center, Chinese Academy of Sciences, Ground-Based Space Environment Monitoring Network (Meridian Project II), Specialized Research Fund for State Key Laboratories.

Availability of data and materials
In this study, atmospheric electric field data can be downloaded from the following website: https://data.ceda.ac.uk. The weather data can be found from the following website: https://www.wunderground.com. The data for the interplanetary magnetic field, solar wind, Dst and other geomagnetic activity parameters can be downloaded from the following website: https://omniweb.gsfc.nasa.gov. Cosmic ray intensity from OULU neutron monitors can be obtained from the following website: http://www01.nmdb.eu/nest. The shocks and ICMEs data can be viewed from the following website: https://izw1.caltech.edu/ACE/ASC/DATA/level3/icmetable2.htm.

Declarations

Competing interests
The authors declare that this research was conducted in the absence of any commercial or financial relationship that could be construed as a potential competing interest.

Received: 27 May 2023 Accepted: 21 September 2023
Published online: 30 September 2023

References
Alemanno F, An Q, Azzarello P et al (2021) Observations of Forbush decreases of cosmic-ray electrons and positrons with the dark matter particle explorer. Astrophys J Letters 920(2):L43
Anisimov SV, Shikhova NM, Kleimenova NG (2021) Response of a magnetospheric storm in the atmospheric electric field of the midlatitudes. Geomag Aeron 61(2):180–190
Blasi P (2013) The origin of galactic cosmic rays. Astron Astrophys Rev 21:70. https://doi.org/10.1007/s00159-013-0070-7
Bothmer V, Daglis IA (2007) Space weather: physics and effects. Springer, Berlin
Cane HV (2000) (1999) Coronal mass ejections and Forbush decreases [C]// Cosmic Rays and Earth: Proceedings of an ISSI Workshop. Springer, Bern, pp 55–77
Guo J (2018) Measurements of Forbush decreases at Mars: both by MSL on ground and by MAVEN in orbit. Astron Astrophys. https://doi.org/10.1051/0004-6361/201732087
Harrison RG (2004) The global atmospheric electrical circuit and climate. Surv Geophys 25:441–484
Harrison RG, Nicoll KA (2018) Fair weather criteria for atmospheric electricity measurements. J Atmos Solar Terr Phys 179:239–250
Jingqun S (1987) Basics of atmospheric electricity. Meteorological Press, Beijing
Kamide Y, Yokoyama N, Gonzalez W et al (1998) Two-step development of geomagnetic storms. J Geophys Res Space Phys 103(A4):6917–6921
Kharayat H, Prasad L, Mathpal R et al (2016) Study of cosmic ray intensity in relation to the interplanetary magnetic field and geomagnetic storms

for solar cycle 23. Sol Phys 291:603–611. https://doi.org/10.1007/s11207-016-0852-y
Kudela K, Storini M, Hofer MY et al (2000) Cosmic rays in relation to space weather. Space Sci Rev 93(1–2):153
Lara A, Gopalswamy N, Caballero-López RA et al (2005) Coronal mass ejections and galactic cosmic-ray modulation. Astrophys J 625(1):441
Le G (2002) Study on the precursor characteristics of the galactic cosmic ray intensity changes before geomagnetic storms. National Space Science Center, Chinese Academy of Sciences, Beijing
Lingri D, Mavromichalaki H, Belov A et al (2016) Solar activity parameters and associated Forbush decreases during the minimum between cycles 23 and 24 and the ascending phase of cycle 24. Sol Phys 291:1025–1041
Nicoll KA (2014) Space weather influences on atmospheric electricity. Weather 69(9):238–241
Oh SY, Yi Y, Kim YH (2008) Globally nonsimultaneous Forbush decrease events and their implications. J Geophy Res Space Phys. https://doi.org/10.1029/2007JA012333
Potgieter MS (2013) Solar modulation of cosmic rays. Living Rev Sol Phys 10:1–66
Rycroft MJ, Israelsson S, Price C (2000) The global atmospheric electric circuit, solar activity and climate change. J Atmos Solar Terr Phys 62(17–18):1563–1576
Rycroft MJ, Harrison RG, Nicoll KA et al (2008) An overview of Earth's global electric circuit and atmospheric conductivity. Planet Atmos Electr 30:83–105
Sanchez-Garcia E, Aguilar-Rodriguez E, Ontiveros V et al (2017) Geoeffectiveness of stream interaction regions during 2007–2008. Space Weather 15(8):1052–1067
Shumilov OI, Kasatkina EA, Frank-Kamenetsky AV (2015) Effects of extraordinary solar cosmic ray events on variations in the atmospheric electric field at high latitudes. Geomag Aeron 55:650–657
Smirnov S (2014) Reaction of electric and meteorological states of the near-ground atmosphere during a geomagnetic storm on 5 April 2010. Earth Planets Space 66(1):1–8
Tacza J, Raulin JP, Mendonca RRS et al (2018) Solar effects on the atmospheric electric field during 2010–2015 at low latitudes. J Geophys ResAtmosp 123(21):11970–11979
Yermolaev YI, Lodkina IG, Nikolaeva NS et al (2014) Influence of the interplanetary driver type on the durations of the main and recovery phases of magnetic storms. J Geophys Res Space Phys 119(10):8126–8136
Zhang J, Richardson IG, Webb DF et al (2007) Solar and interplanetary sources of major geomagnetic storms (Dst100 nT) during 1996–2005. J Geophys Res Space Phys. https://doi.org/10.1029/2007JA012321

Publisher's Note